Optical magnetic circular dichroism in the canted antiferromagnetic α-Fe_2O_3: bulk single crystal and nanocrystals

R. Ivantsov, O. Ivanova, S. Zharkov, M. Molokeev[1,2], A. Krylov, V. Temerov, I. Edelman
[1] Kirensky Institute of Physics, Federal Research Center KSC SB RAS, Krasnoyarsk 660036, Russia
[2] Siberian Federal University, Krasnoyarsk, 660041, Russia

α-Fe_2O_3 is a canted antiferromagnetic with a Neel temperature of T_N = 960 K and undergoing the Morin transition at 260 K when the sublattice magnetic moments become antiparallel and the resulting magnetic moment disappears. Due to the variety of magnetic properties and a wide range of applications, this material still remains in the top list of the physics of magnetic phenomena. In order to understand the features of magneto-optical effects in α-Fe_2O_3 we carried out the detail investigation of the optical magnetic circular dichroism (MCD) for the α-Fe_2O_3 nanoparticles in comparison with the α-Fe_2O_3 single crystal optical and magneto-optical parameters obtained with the ellipsometric method. Based on the analysis of the MCD spectra measured directly for nanoparticles and calculated from ellipsometric data for single crystal, two types of the features were identified describing by the Gaussian and S-shape lines. Very strong S-shape line observed at 2.0-2.5 eV appeared to be an exceptional feature of α-Fe_2O_3 distinguishing it from other iron oxide compounds. It is shown that the MCD originates from the weak d-d transitions, including, pare exciton-magnon transition, while optical absorption is associated primary with the charge transfer transitions.

Key words: Hematite, α-Fe_2O_3, optical absorption, magnetic circular dichroism, d-d transitions, ellipsometric method

1. Introduction

Hematite, α-Fe_2O_3, occupies a very special place among all magnetic materials. Despite the many applications in various fields of human activity, starting from ancient times, and more than two centuries of research history, it still attracts the attention of researchers and engineers and continues to set puzzles. Start to study of the hematite magnetic properties goes back to the works of J. Kunz [1] and T. Smith [2,3], who revealed a weak magnetic moment of this mineral in spite of the antiferromagnetic spin ordering. Morin's discovery of the magnetic transition with the disappearance of the total magnetic moment at the crystal cooling lower ~260 K called later the Morin temperature T_M [4] was an important stage in the study of the hematite magnetic properties. Shull with co-authors [5] has demonstrated with the neutron diffraction that antiferromagnetic

ordered spins were directed along the trigonal or *c*-axis of the rhombohedral α-Fe_2O_3 structure at temperatures below T_M. When the sample heating above T_M, spins flop to the basal *c*-plane and become canted out of exact antiparallel directions. The canting is of about several degrees. In 1957, I. Dzialoshinskii has developed thermodynamic theory of the origin of the weak ferromagnetism in antiferromagnetic substances with a specific magnetic structure [6]. He showed this ferromagnetism to be due to the competition between the relativistic spin-lattice interaction and magnetic dipole interaction. Different temperature dependences of the interactions can lead to magnetic phase transitions, in particular, to the Morin transition in hematite. The Morin temperature, magnetic and other physical properties of hematite can be affected strongly by size effects, pressure, lattice strains, random or targeted impurities and so on [7,8,9,10,11]. Such variability in the properties of hematite is one of the reasons why researchers have continued interest in this material.

The study of the optical properties of a substance is important not only in view of possible applications, but also because optical and, especially, magneto-optical spectroscopy provide valuable information about the structure of excited states and electronic transitions between them. As concerns α-Fe_2O_3, its very high optical density in visible and UV spectral regions did not allow the absorption measurements of bulk samples in transmitted light and most of the investigations of optical characteristics were carried out with the diffuse reflection using α-Fe_2O_3 powder, or with nanoparticles dispersed in any liquid, or with thin films. Sherman and Waite [12] analyzed the diffuse reflectance spectrum recorded in [13] for the sintered hematite pellets of the Mapico Inc. Co. (St. Louis, USA). They assigned maximum centered near 2.88 eV (430 nm, 23000 cm^{-1}) to the fundamental absorption band and a series of very weak features on the background of this absorption were ascribed to the one-ion crystal field (CF) d-d transitions and some of them to the double exciton-magnon (EM) transitions in the Fe^{3+} ions in accordance with the Tanabe-Sugano diagram [14].

Diffuse reflectance spectra of α-Fe_2O_3 nanoparticles were studied in Ref. [15] to reveal the finite size effect. Two lowest bands at E=1.43 eV, E=1.8 eV observed at a little different energies comparing to [12] were assigned to the CF, and band at E=2.22 eV was compared with EM transition, analogously to [12]. Non-monotonous increase of the energy of EM transition with the nanoparticles size (d) decrease was shown, especially strong for d<20 nm. Optical spectra of the chemically synthesized α-Fe_2O_3 nanocrystals of different size and structural modifications (hexagonal, *R*3*c*, and corundum) dispersed in ethanol were studied and analyzed in Ref. [16]. Identification of the optical spectra features was similar to that presented in the above cited references, and the size effect on the transition

energy has revealed itself also for the EM transition. Mitra with co-workers [17] and Chakrabarty and Chatterjee [18] measured optical absorption of the hematite nanocrystals of different morphology synthesized by the solvo-thermal method (for optical measurements nanocrystals were dispersed in the spectroscopic grade ethanol). They revealed the noticeable effect of the nanocrystal morphology in the absorption spectrum. At that, spectrum of the rhombohedral shape nanoparticles was very close to data of [12], and features in the spectrum were associated with the same CF transitions.

Marusak et al. studied optical absorption of the α-Fe_2O_3 thin films prepared by the radio-frequency magnetron sputtering in the region of 250-959 nm and of the very thin α-Fe_2O_3 single crystal in the region of 700-1000 nm, that is, in the region of the first CF transition $^6A_{1g} \rightarrow {}^4T_{1g}$ (^4G) [19]. In the last case they have measured for the first time the temperature behavior of the peak shape and intensity. Later, Jõgi et al. [20] have received optical absorption spectrum for hematite film of 50 nm thick deposited at 400 °C at quartz substrate using hybrid process of atomic layer deposition and pulsed chemical vapor deposition (ALD/pulsed CVD). The spectrum shape was similar to that published in [12], but spectral maxima were approximately 100 nm shifted to the higher energies.

New approach to the interpretation of the hematite optical spectrum has been suggested quite recently [21]. At variance with the above mentioned studies considering this spectrum to be due to the Fe^{3+} one-ion d-d transitions, the author of [21] worked out the many-body perturbation theory, including the effects of electron-hole interaction, that provided good agreement with absorption measurements available in literature and associated the hematite absorption spectrum mostly with the ligand-to-metal charge transfer excitations, giving rise to fairly localized excitons.

What concerns magneto-optical properties, several articles are available in literature devoted to observation of the α-Fe_2O_3 crystal domain structure with the magneto-optical Faraday or Kerr effects [22,23,24]. Besides, several authors used magnetic linear birefringence to study Morin transition in hematite [25,26,27]. Krinchik with co-authors have measured transvers Kerr effect and calculated off-diagonal components of the dielectric tensor for the α-Fe_2O_3 bulk single crystal [28,29,30]. They have revealed a series of peaks in the Kerr spectra and have underlined the role of the surface states in the formation of the magneto-optical spectra [29]. Balasubramanian with co-authors studied the magnetic field dependencies of the longitudinal Kerr Effect at 638 nm to characterized the α-Fe_2O_3 nanoparticles coated on a quartz substrate [31]. To our best knowledge, data on the hematite magneto-optical spectra in the transmitted light, that is, Faraday rotation (FR) and magnetic circular dichroism (MCD) are absent in literature. At

the same time these effects are exceptionally informative for the deep understanding of an origin of the electron transitions forming optical and magneto-optical spectra of a substance. The absence of the data on these effects for hematite is due, partly, to the very high optical density of the crystal.

Here we made an attempt to comprehensively study the magneto-optical spectra and optical characteristics of hematite using both an ensemble of nanoparticles and a bulk single crystal of this compound. The magnetic circular dichroism, Faraday rotation and optical absorption spectra were recorded in the transmitted light for the α-Fe_2O_3 nanocrystals. Transverse Kerr effect (TKE) and optical constants for the α-Fe_2O_3 bulk single crystal were measured in the reflected light with the help of the magneto-ellipsometric device.

2. Experimental

Hematite nanoparticles (α-Fe_2O_3) were synthesized by chemical deposition from a solution. Synthesis of nanoparticles was carried out at room temperature and constant stirring by dropwise adding an aqueous solution of ammonia (15 vol.%) to an aqueous solution of iron (III) chloride (1 wt.%). The precipitate was washed with distilled water. The α-Fe_2O_3 single-crystal was grown in the solution-melt: 79%wt. [Bi_2O_3 + 1.1Na_2O + 2.2B_2O_3] + 21%wt. Fe_2O_3 in the temperature range from 1075-1042 °C with an increasing rate of 1-4 °C/day.

To characterize nanoparticles structure, the powder diffraction data for Rietveld analysis were collected at room temperature with a Bruker D8 ADVANCE powder diffractometer (Cu-Kα radiation) and linear VANTEC detector. The step size of 2θ was 0.016°, and the counting time was 5 s per step. Rietveld refinement was performed by using TOPAS 4.2 [32].

Morphology, structure and elemental composition of the nanoparticles were investigated using transmission electron microscope (TEM) JEM-2100 (JEOL Ltd.) operating at the accelerating voltage of 200 kV. Selected-area electron diffraction (SAED) was used to determine the structure of the nanoparticles.

The nanoparticles were also characterized by Raman spectroscopy. During collection of the Raman spectra, a low laser power of ~0.8 mW was used.

To carry out the MCD, FR, and optical absorption measurements, transparent composite plates containing the nanoparticles were prepared as it was described in [33]. The nanoparticles powder was mixed with dielectric transparent silicon-based glue (“Rayher” art. no. 3338100 80 ml) in the weight proportion 0.5:100 and measures were undertaken to obtain the homogeneous particles distribution using an ultrasonic bath. The mixture was placed between two thin

glass plates spaced by wires 0.15 mm in diameter and solidified. The low magnetic powder concentration allowed us to exclude the interaction between nanoparticles.

The optical density spectra we recorded at 300 and 80 K with the laboratory made dual beam spectrometer.

MCD and FR were measured in the normal geometry: the magnetic vector and the light beam were directed normal to the samples plane. The modulation of the light wave polarization state from the right-hand to the left-hand circular polarization relatively to the magnetic field direction was used for the MCD measurements. The MCD value was measured as the difference between the sample optical density for right and left polarized light waves ($\Delta D=D_+-D_-$) in the spectral range of 1.2–3.2 eV in a magnetic field 13 kOe at the temperatures 80-300 K. The modulation of the polarization plane of the linearly polarized wave was applied when measuring FR which value was determined as a rotation of the light wave polarization plane when reversal the sample magnetization. The measurement accuracy was about 10^{-4} for MCD and 0.002 degrees for FR, the spectral resolution was 20–50 cm^{-1} depending on the wavelength.

The TKE and optical parameters spectra were obtained for the light reflected from the (001) face of the bulk single crystal using the magneto-optical ellipsometer “Ellipse 1891” [34, 35]. The light incidence angle was 70 degrees, magnetic field up to 4.0 kOe was directed parallel to the (001) crystal plane. At that, ellipsometric parameters ψ and δ as well as their changes in the magnetic field $\Delta\psi$ and $\Delta\delta$ were measured in the spectral region of 1.2–4.9 eV with an accuracy of $2*10^{-3}$. Absorption and refractive indexes, k and n, as well as the real and imaginary parts of the diagonal component of the dielectric tensor were calculated according to [35]. Off-diagonal (real and imaginary parts) components and TKE were calculated using an approach suggested in [36].

3. Results and discussion

XRD spectrum of nanoparticles is shown in Fig. 1. XRD peak positions indicated in the Figure match the rhombohedral symmetry in agreement with data from literature [37, 38,39]. Rietveld refinement was stable and gave low *R*-factors (R_{wp} = 1.20 %, R_p = 0.91 %, R_{Bragg} = 1.26 %). The cell parameters were found to be *a*=5.0359(4), *c*=13.753(1) Å, and the average crystalline size d= 62.9(9) Å.

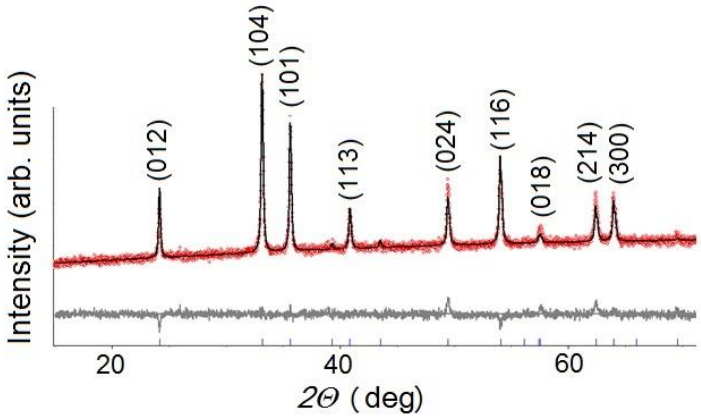

FIG. 1. Difference Rietveld plot of α-Fe_2O_3 powder sample. **Максим, может стоит вставить для монокристалла? (Нет, это же порошковые данные, монокристалл если и существовал, то он был разрушен. Тут все нормально.)**

The TEM images of nanoparticles are presented in Fig. 2. The nanoparticles are of irregular rounded shape and demonstrate the rather wide size dispersion. The average particles size was estimated as 30 nm. All interplanar distances obtained from the SAED pattern coincide with data of [40].

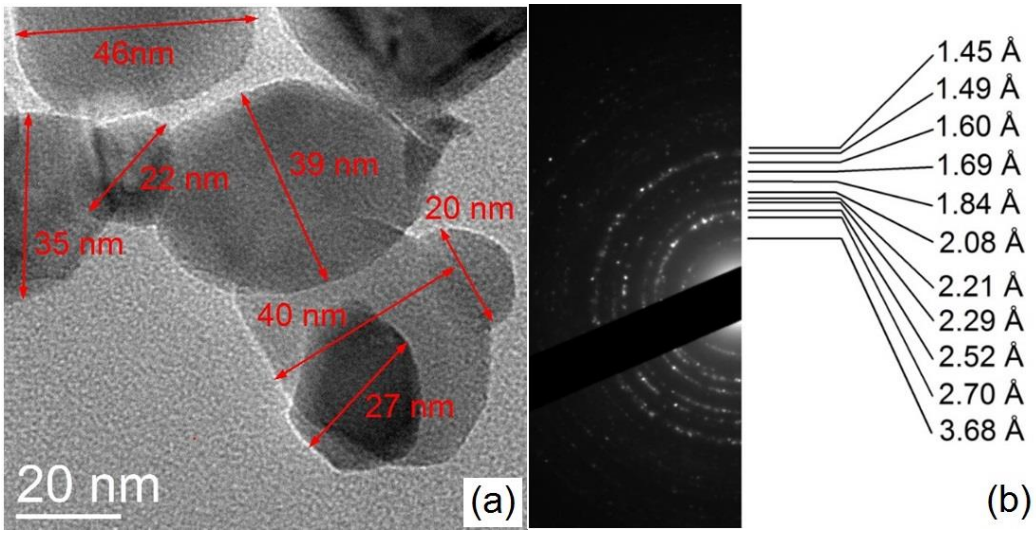

FIG 2. TEM image of α-Fe_2O_3 nanoparticles (left) and SAED pattern with the interplanar distances (right).

Raman spectra of different portions of the α-Fe_2O_3 powder are shown in Fig. 3. The close coincidence of the spectra evidences on the powder homogeneity. Six close located lines at ~218, 240, 285, 410, 487, 601 and one very strong at ~ 1311 cm^{-1} characteristic for hematite [41, 42, 43] are clearly seen in the Raman

spectrum. In Ref. [41], lines at 225, 245, 291, 411, 500, 611, and 1321 cm^{-1} were observed in Raman spectra of synthetic hematite crystal. In the case of hematite nanoparticles, some of the observed lines were a little bit shifted: 225 (A_{1g}), 241 (E_g), 291 (E_g), 409 (E_g), 496 (A_{1g}) and 608 (E_g) cm^{-1} [42] comparing to bulk crystals which is common for nanoparticles [44]. Here, symbols in brackets refer to the phonon symmetry. The additional bands between 600 and 1300 cm^{-1} might be associated with impurities analogously to that how way similar lines were explained in [41]. The intense feature at 1311 cm^{-1} corresponds to the analogously line in the Raman spectrum of the α-Fe_2O_3 powder sample observed in Ref [45] at 1320 cm^{-1} that was assigned to a two-magnon scattering arising because the exchange interaction between the antiparallel magnetized ions.

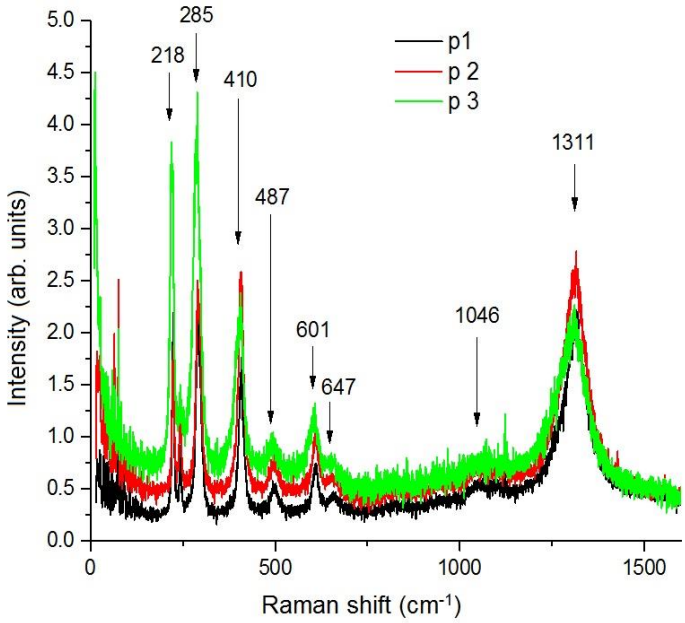

FIG 3. Raman spectra for different portions of the α-Fe_2O_3 powder.

Thus, Raman spectra confirmed the structure data presented above evidence on the rather high crystalline quality of the α-Fe_2O_3 nanoparticles, and one can expect the close coincidence of their optical and magneto-optical properties with that of bulk single crystal.

MCD spectrum of the composite sample containing α-Fe_2O_3 nanoparticles together with FR and absorption spectra recorded at room temperature are presented in Fig. 4. Magnetic field and the light propagation directions were perpendicular to the sample plane. The values of MCD and FR are given to the effective thickness of hematite nanoparticles, which was determined as follows. The total mass of nanoparticles introduced into the composite sample was divided into the specific mass of hematite, which gave a total volume of particles. The resulting value was then divided by the sample area. Thus, the effective thickness of the nanoparticles layer was obtained under the assumption that they are evenly

distributed over the sample area and that the specific gravity of the nanoparticles corresponds to the specific mass of hematite. The hematite specific MCD at the maximum at 3 eV thus estimated is approximately twice as small as the corresponding maximum in the MCD spectrum of yttrium-iron garnet (See Fig. 5 in [46]).

A series of strong peaks is seen in the MCD spectrum which positions correspond to the weak features in the absorption spectrum. FR and MCD spectra correlate with each other in the region of 2.1-2.4 eV (highlighted in Fig. 4 a by vertical dashed lines). The S-shape MCD feature corresponds to the U-shape FR line. Such a situation can occur in the case when two electron transitions are excited at close energies by the electromagnetic waves with the opposite circular polarizations, for example, in the case when electric dipole transitions will occur simultaneously in the neighboring exchange-coupled ions between ground and excited states accompanied by magnetic dipole transitions between sublevels of the ground state. Such a process is characteristic for the antiferromagnetic substances and it is called a double or exciton-magnon transition.

Comparison is worth of MCD spectrum with spectra of ferrimagnetic compounds containing only one type of the d-ion, namely, Fe^{3+} ions – $Y_3Fe_5O_{12}$ [46] and γ-Fe_2O_3 [47] presented in literature. Two strong maxima are observed at energies 2.58 and 2.79 eV for $Y_3Fe_5O_{12}$ and at 2.3 and 2.6 eV for γ-Fe_2O_3. In the first case, the maxima are very well resolved while in the second case they are somehow overlapped. Similar two overlapping maxima are observed here for α-Fe_2O_3 at the same energy interval 2.55-3.0 eV. At energies lower 2.3 eV the MCD signal decreases sharply for both compounds γ-Fe_2O_3 and $Y_3Fe_5O_{12}$. Analogous picture was presented by Kahn, Pershan, and Remeika, who studied polar Kerr effect associated with the F^{3+} ions in the rare-earth orthoferrites: strong negative maximum corresponded to ~3 eV and, at the electromagnetic wave energies lower than 2.5 eV, Kerr effect signal practically disappeared [48]. At the same time, in the α-Fe_2O_3 spectrum very strong MCD S-shape signal is observed covering the whole interval 1.5-2.5 eV.

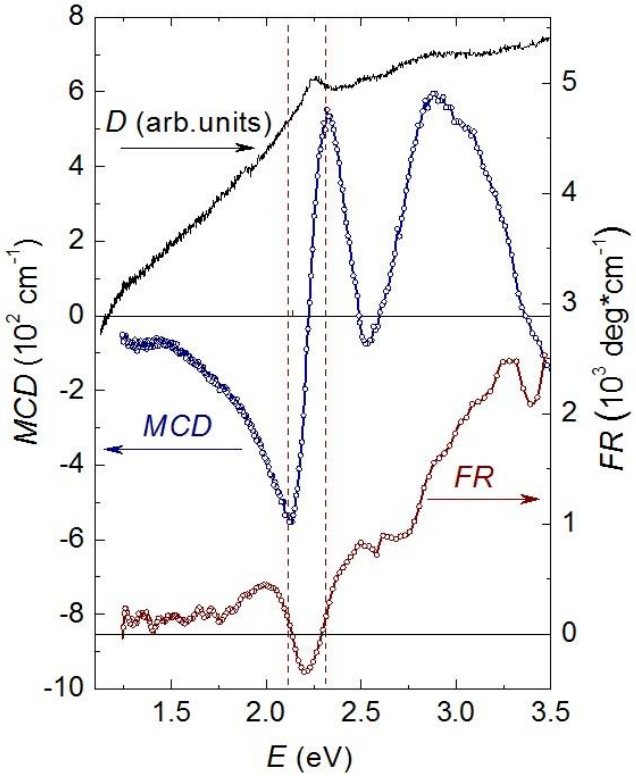

FIG. 4. The MCD, FR and absorption spectra of α-Fe_2O_3 nanoparticles dispersed in the silicon matrix at room temperature. Magnetic field H=1.3 T.

Before comparing the magneto-optical spectra for nanoparticles with that for a single crystal, we present the MCD temperature dependence for nanoparticles. The characteristic feature of hematite is the so called Morin phase transition when, at the temperature decrease, the antiferromagnetic vector changes its orientation from the c-basal plane to the c-axis and the spin canting disappears at T_M and, as a consequence, the net magnetic moment and, consequently, MCD becomes equal to zero, because MCD is linear function of magnetization. Figure 5 shows several MCD spectra of the sample with nanoparticles recoded at different temperatures and the temperature dependence of the strong MCD peak intensity determined as the square under the curve in the spectral interval 2.6-3.4 eV which confirms the Morin transition in the nanoparticles. The transition is extended over a wider range of temperatures comparing to the literature data for α-Fe_2O_3 single crystal [4]. It starts at 260 K analogously to bulk samples and then decreases, first quickly (up to ~230 K), and then slower. At temperature lower than 200 K, the MCD signal becomes very small for the correct measurements. Similar magnetization changes were observed for small α-Fe_2O_3 particles in [7]. As a whole, the MCD temperature dependence indicates proximity of nanoparticles properties and properties of the bulk hematite crystal known in literature.

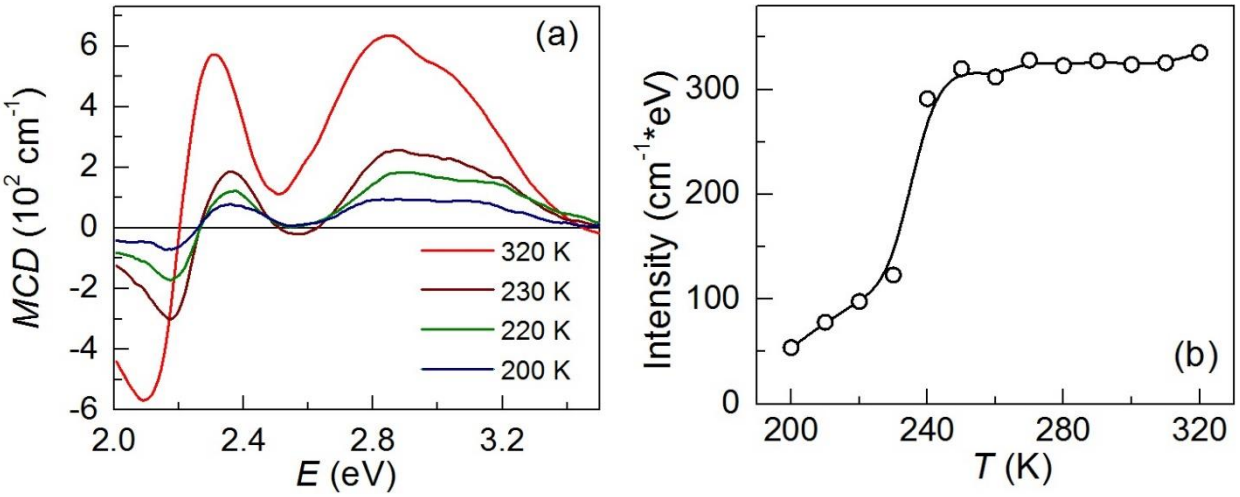

FIG. 5. MCD spectra of the α-Fe_2O_3 nanoparticles dispersed in the silicon matrix recoded at different temperatures (a) and the integral intensity of the MCD signal in dependence on temperature (b). Magnetic field H=0.35 T.

Turn now to the optical and magneto-optical spectra of the α-Fe_2O_3 single crystal calculated from the ellipsometric parameters (Ψ and Δ) measured with the magneto-optical ellipsometer [34] for the light reflected from the (001) face of the crystal. Here, Ψ is the ratio of the reflection coefficients for components of the electromagnetic wave polarized parallel and perpendicular to the light incidence plane, r_p and r_s, correspondingly, and Δ is the phase shift between these components. These parameters determine the complex reflection coefficient

$$\rho = \frac{r_p}{r_s} = tg\Psi e^{i\,\Delta}\ , \qquad (1)$$

which allows determining the complex refraction index η of a medium [36]

$$\eta = sin\varphi\sqrt{1 + tg^2\varphi\left(\frac{1-\rho}{1+\rho}\right)^2}, \qquad (2)$$

where φ is the angle of the light incidence to a sample. Measuring Ψ and Δ at two opposite directions of external magnetic field, one can determine $\eta_{\pm}$ with Eq. (2) and components of the complex dielectric tensor ε written as

$$\varepsilon = \begin{pmatrix} \varepsilon_{xx} & \varepsilon_{xy} & 0 \\ \varepsilon_{yx} & \varepsilon_{yy} & 0 \\ 0 & 0 & \varepsilon_{zz} \end{pmatrix} \qquad (3)$$

for the samples magnetized to saturation in a magnetic field parallel to the positive z-axis direction in a right-handed set of axes. For simplicity, diagonal components were taken to be equal with each other $\varepsilon_{xx} = \varepsilon_{yy} = \varepsilon_{zz} = \varepsilon$, and $\varepsilon_{xy} = -\varepsilon_{yx} =$

$-ig$. The right and left circular polarized components are the normal mods of the waves propagating along the positive z-axis in such a system. The real and imaginary parts of the dielectric tensor components $\varepsilon = \varepsilon' - i\varepsilon''$ and $g = g' - ig''$ are related to the complex refractive index $\eta_{\pm} = n_{\pm} - ik_{\pm}$ for the right (+) and left (-) circular polarized waves by the following expressions: $\eta_{\pm}^2 = \varepsilon \mp g$.

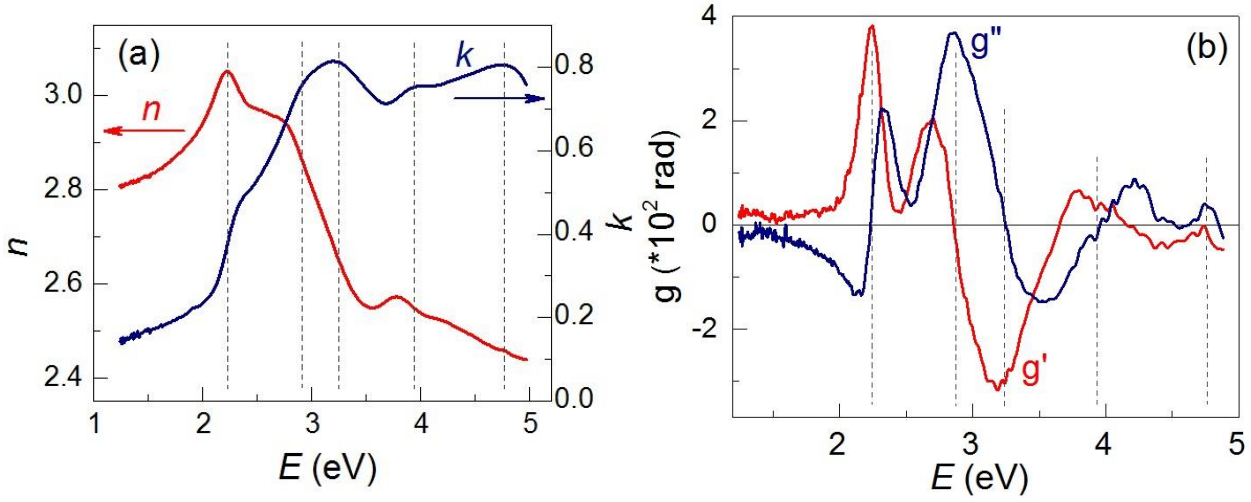

FIG. 6. Spectral dependencies of the refraction index (n) and absorption coefficient (k) of the α-Fe_2O_3 single crystal for the light reflected from the (001) crystal plane (a) and off-diagonal components g' and g'' of the dielectric tensor (b).

Spectral dependencies of the refraction index (n) and absorption coefficient (k) of the α-Fe_2O_3 single crystal obtained from the measurement in zero magnetic field are presented in Fig. 6 a. Some divergences are seen between the *k* spectrum and the nanoparticles absorption spectrum (Fig 4). Peak near 2.2 eV is more distinct in the case of nanoparticles while the peak centered at 3.2 eV is more prominent for the single crystal. Besides, the higher energy peaks at 3.9 and 4.85 eV are seen at the measurements in the reflected light. In this region nanoparticle sample is quite opaque. The redistribution of the 2.2 eV and 3.2 eV absorption peak intensities was observed for the α-Fe_2O_3 nanoparticles as their size increased from 5 to 48 nm (Fig.9 in [16]). Similar results were presented in [15]. On the other hand, absorption spectra for the α-Fe_2O_3 crystals and films available in literature [12, 19] are close to the *k* spectrum shown in Fig. 6 a.

Spectra of the calculated off-diagonal components g' and g'' for α-Fe_2O_3 single crystal are presented in Fig 6 b. Fig. 7 shows the MCD spectrum (curve 1) of the single crystal calculated using the g' and g''spectra

$$\theta = \frac{4\pi}{\lambda}\left\{\frac{n}{k^2+n^2}g'' - \frac{k}{k^2+n^2}g'\right\}. \qquad (4)$$

Experimental MCD spectrum of α-Fe_2O_3 nanoparticles is shown in Fig. 7 (curve 2) also for comparison. Extrema positions in both curves are the same. Similar to the redistribution of the absorption peak intensities near 2.2 and 3.0 eV, the ratio of the MCD peak intensities changes at the transition from nanoparticles to single crystal. Similar to the absorption spectrum, several higher energy peaks are seen in the single crystal MCD spectrum.

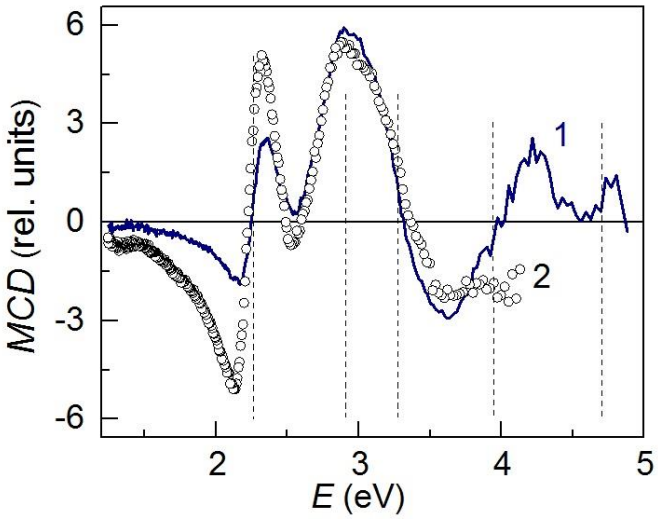

FIG. 7. MCD spectra calculated for the α-Fe_2O_3 single crystal from the ellipsometric data (curve 1) and measured directly for α-Fe_2O_3 nanoparticles (curve 2).

Both optical absorption and the MCD spectra features can be due to several electron transitions in a medium. Lenglet with co-authors analyzing optical and FR spectra of mixed ferrite-garnets and ferrite-spinel's [49], considered one-ion CF d-d electron transitions in the Fe^{3+} ions, charge transfer transitions between Fe^{3+} ions occupying opposite sublattices, and charge transfer transitions between Fe^{3+} and ligands as main types of transitions responsible for magneto-optical effects. The 1–2 eV interval was associated with d-d transitions in octahedral Fe^{3+} ions. More complicated situation takes place at higher energies (2–4 eV). Here, d-d transitions from the ground to the exited states of octahedral Fe^{3+} can overlap with the transitions of other nature. As it was mentioned in the introduction, an essential contribution to absorption and magneto-optical spectra is associated with so-called pare transitions in the exchange-coupled Fe^{3+} ions when electro dipole transitions from the ground to the exited states and magneto dipole transitions between the ground state components splitted by magnetic field occur simultaneously in both ions. In this case, the transition energy is approximately equal to the sum of two single ion Fe^{3+} d-d transitions [50]. From this point of view, it seems to be interesting to mention results of papers [50, 51], where absorption spectra of the

Fe^{3+} impurity ions substituting partly the Al^{3+} ions in Al_2O_3 crystal isostructural to α-Fe_2O_3. When the iron concentration in Al_2O_3 crystal was very low, of about 0.1 at. %, only d-d transitions in Fe^{3+} were observed which fitted excellently to the Tanabe-Sugano diagram [14]. Increasing of the Fe^{3+} concentration up to 1 at. % led to an appearance of the additional peaks in the absorption spectrum which were ascribed to the pare transitions $2(^6A_{1g}(^6S))\rightarrow 2(^4T_{1g}\ (^4G))$ at ~2.2 eV, $2(^6A_{1g}(^6S))\rightarrow {}^4T_{1g}(^4G)+{}^4T_{2g}\ (^4G)$ near ~2.9 eV, $2(^6A_{1g}(^6S))\rightarrow {}^4A_{1g}, {}^4E_g\ (^4G)+{}^4T_{1g}$ (^4G) at ~3.7 eV. At that, absorption maxima associated with the first and third transitions are rather insensitive while the second transition contribution is almost invisible. In principle, features associated with transitions of this type should be observed more clearly in the stoichiometric α-Fe_2O_3 crystal.

In the absorption and MCD spectra of many iron oxides [46,47], two features in the lower part of the spectrum (1-2 eV) due to the d-d electron transitions $^6A_{1g}(^6S)\rightarrow {}^4T_{1g}\ (^4G)$ and $^6A_{1g}(^6S)\rightarrow {}^4T_{2g}\ (^4G)$ were observed distinctly. As, energies of these transitions depend strongly on the CF value, they are critical for the determining of the CF parameters and identification of the higher energy spectral features with the definite CF transitions. However, the absorption spectrum of nanoparticles and *k* spectrum of single crystal (Figs. 4, 6, correspondingly) demonstrate, practically, no features in this interval, possibly, they are not seen on the background of the intensive tail of the higher energy transitions.

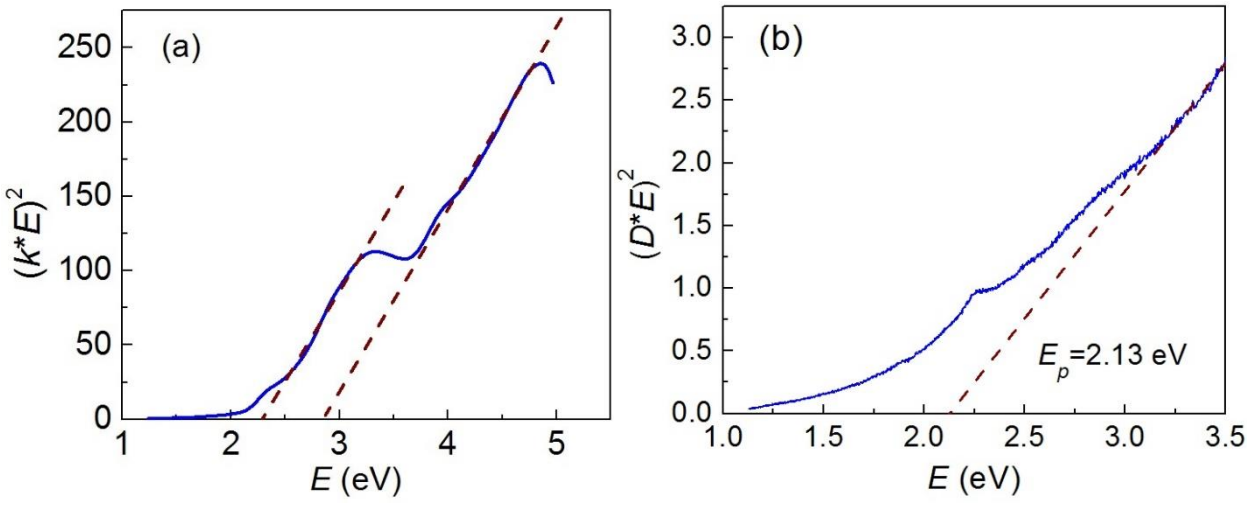

FIG. 8. Tauc's plots with a linear extrapolation of the quantity $(kE)^2$ (a) and $(D*E)^2$ (b) for α-Fe_2O_3 single crystal and nanoparticles, correspondingly.

To analyze the absorption spectra we used the Tauc equation [52]: the absorption band gap Eg of a medium can be determined by

$$kh\gamma = (h\gamma - E_g)^n, \qquad (5)$$

where hν is the photon energy, *k* (небольшая путаница с волновым вектором, может для коэффициента выбрать другую букву, например C?)is the absorption coefficient (or the optical density) and n is either 1/2 for the direct transition or 2 for the indirect transition. An extrapolation of the linear p[art of the plot gives the value of the band gap as the intercept to the x-axis. Figure 8 shows the Tauc plots of *k* spectrum (Fig. 6a) of α-Fe_2O_3 single crystal (a) and of absorption spectrum (Fig. 4) of nanoparticles (b) for n=1/2 analogously to that as it was done in Ref [53]. In the first case, two linear parts of the plot gave two meanings of the band gap E_g =2.25 and E_g =2.8 eV. For nanoparticles only lower band gap is observed because of high optical density of the sample at energies E>3.5 eV, and linear part of the Tauc plot gave the band gap 2.13 eV, that is very close to the band gap value for the single crystal. Two sets of band gaps in Tauc plot was observed in [53] for the Fe_2O_3 nanoparticles synthesized by the laser ablation method at different laser energies. The lower and the higher energy band gaps were observed at the energy intervals (2.16–2.28 eV) and (2.68–3.10) eV in dependence on the synthesis condition. Authors of Ref. [53] identified the lower energy band gap with both the pare excitations and the inter-valence charge transfer transitions between iron ions in the opposite spin direction sublattices, while the higher energy band gap was ascribed to inter-valence charge transfer and charge transfer between O^{2-} and Fe^{+3}. Using the gap values obtained for single crystal, one can estimate contributions of transitions responsible for these gaps and subtract them from the experimental curve. The lower energy part of the absorption spectrum obtained after this procedure is shown in Fig. 9. Two maxima centered at 1.4 and 1.9 eV are seen which can be attributed to transitions $^6A_{1g}(^6S)\rightarrow{}^4T_{1g}$ (^4G) and $^6A_{1g}(^6S)\rightarrow{}^4T_{2g}$ (^4G) what coincides very well with results of Ref. [54] where absorption of the thin slice of the α-Fe_2O_3 single crystal was investigated at 4.2 K with high resolution. At room temperature, the band at 1.9 eV was not observed in [54] like to our room temperature spectra (Figs. 4 and 6).

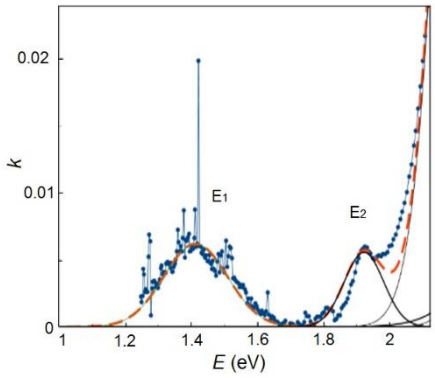

FIG. 9. Low energy part of the absorption coefficient obtained after subtracting of higher energy contributions from the initial *k* curve.

As it was mentioned in the Introduction, Piccinin [21] has performed the first principal calculations of the α-Fe_2O_3 band structure using many-body perturbation theory, including the effects of electron-hole interaction by solving the Bethe-Salpeter equation. Based on the obtained band structure, the diagonal components ε'_{xx} and ε''_{xx} of the α-Fe_2O_3 dielectric function was calculated and the results was compared with the experimental data on the α-Fe_2O_3 absorption spectrum available in the current literature [55, 56]. The absorption maximum in the vicinity 2.2-2.3 eV was interpreted as the first optically allowed transition which was due to formation of localized excitons associated, mainly, with the transition from the top of the valence band to the bottom of the conduction band. Such a transition should be of the ligand-to-metal charge transfer type because the valence band comes from a hybridization between O 2p and Fe 3d states while the conduction band is determined by the Fe 3d states. Tauc's plot built in Ref. [21] coincides with that presented here in Fig. 8.

In Ref. [21], the difference is discussed also between this maximum intensities for the light wave polarized parallel or perpendicular to the crystal *c*-axis. In particular, the shape of the ε''_{xx} spectrum obtained with the BSE@PBEO calculations (Bethe-Salpeter Equation @ Perdew–Burke-Ernzerhof) for the light wave electric vector E parallel to the c-axis (Fig. 8 in [21] is very close to the ε''_{xx} spectrum shape of α-Fe_2O_3 single crystal obtained with the ellipsometric method (Fig. 10). Now, one can explain the difference between details of the absorption and MCD spectra of the single crystal and of nanoparticles. At the conditions of the ellipsometric measurements only one orientation of the E vector close to be parallel to the c-axis was used. In the case of nanoparticles, their crystal axes are oriented randomly in a sample and, thus, for the part of particles vector c is oriented perpendicular to c-axis providing higher contribution of the transition discussed into absorption spectrum. So, our experimental data on the absorption and the dielectric tensor components of the α-Fe_2O_3 single crystal and nanoparticles correlate well with the predictions of the theory developed in [21].

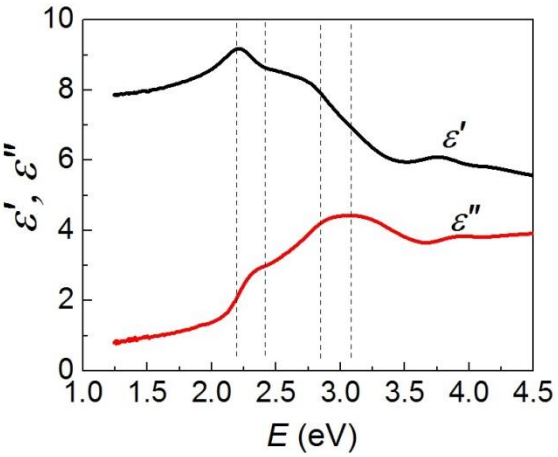

FIG. 10. Real (ε') and imaginary parts (ε'') of the diagonal component of the dielectric tensor of the α-Fe_2O_3 single crystal obtained with the ellipsometric measurements.

To identify features observed in the α-Fe_2O_3 magneto-optical spectra with the specific electron transitions in the Fe^{3+} ions we carried out the decomposition of g'' spectrum to the components. Comparing of this spectrum with *k* spectrum (compare Figs. 6a and 6b) shows that energies of several maxima in g'' and *k* spectra coincide while maxima in *k* spectrum at several energies correspond to the inflection points in g'' spectrum. Taking into account this circumstance, best fit of the sum of the decomposition components to the g''spectrum (Fig.11) was obtained with four Gaussian lines (E_1, E_2, E_4, E_5) and three derivatives (E_3, E_6, E_7). As g'' spectrum determines the MCD spectrum and these two spectra coincide, practically (compare Figs. 6 b and 7), the g'' spectrum decomposition can be applied to the MCD spectrum. Energies corresponding to the gravity centers of the E_1, E_2, E_4, E_5 lines match very well to the Tanabe-Sugano diagram (Fig.12). Therefore, MCD observed at these energies should be attributed to the transition between ground and excited 3d states splitted by the magnetic field which intensity is determined by the difference in spin population of the ground state sublevels. This statement is confirmed by the MCD temperature dependence (Fig. 5).

The S-shape of the MCD features at E_3, E_6, E_7 can be associated with the excitons-magnon mechanism of the light absorption by two neighboring 3d ions taking off partly the forbiddance of d-d transitions.

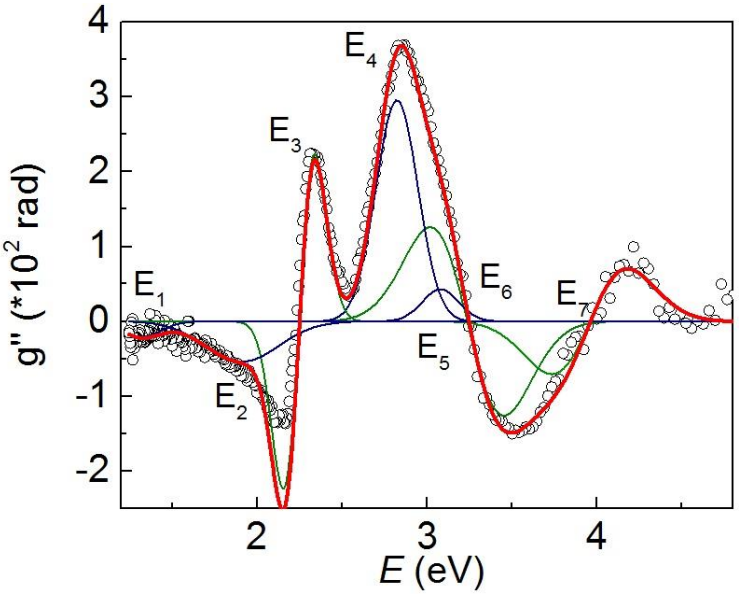

FIG. 11. The g'' spectrum decomposition to the Gaussian and Gauss derivative components. E notation shows the gravity centers of the corresponding absorption features.

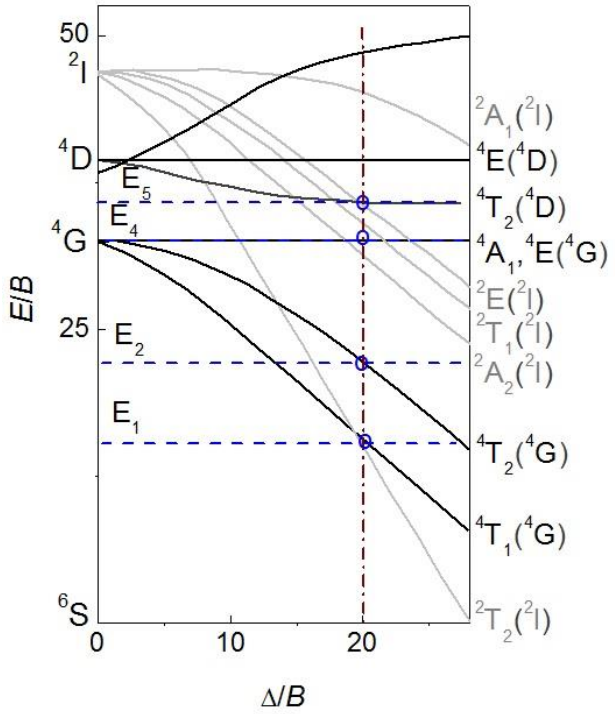

Fig. 12. Tanabe-Sugano diagram for high-spin Fe^{3+} in octahedral coordination. The state energies were calculated using the g'' spectrum decomposition.

Most intense S-shape feature at ~2.2 eV consists of two peaks of the opposite signs, with the distance between their gravity centers equal to ~1600 cm^{-1}, what is close to the energy of the two-magnon peak observed in the Raman spectrum 1311 cm^{-1} (Fig. 3). The distance between two excitons should not be equal exactly to two magnon shift in the Raman spectrum because other processes like phonon can

be involved into transition. Other two transitions which we ascribed to pare transitions too overlap with the one-ion transitions and look not so distinct. Energies of the g'' decomposition components and their identification with crystal field transitions are presented in Table 1 in comparison with data of several authors obtained from the analysis of the α-Fe_2O_3 thin films absorption and the α-Fe_2O_3 powder diffuse reflectance spectra.

Table 1. Energies (eV) of the g'' decomposition components (E_1-E_7) and the components identification with CF and pare transitions comparing to the results of other authors

	Electron transition	This research	[51]	[12]	[57]*	[18]
E_1	$^6A_{1g}(^6S)\rightarrow{}^4T_{1g}(^4G)$	1.4	1.17	1.4		
E_2	$^6A_{1g}(^6S)\rightarrow{}^4T_{2g}(^4G)$	1.92	1.78	1.91		
E_3	$2(^6A_{1g}(^6S))\rightarrow 2(^4T_{1g}(^4G))$	2.24	-	2.34	2.21	2.18-2.23
E_4	$^6A_{1g}(^6S)\rightarrow{}^4A_{1g}, {}^4E_g(^4G)$	2.83	2.76	2.79	2.76	2.7-3.03
E_5	$^6A_{1g}(^6S)\rightarrow{}^4T_{2g}(^4D)$	3.11	3.13	3.06	3.22	
E_6	$2(^6A_{1g}(^6S))\rightarrow{}^4T_{1g}(^4G)+{}^4T_{2g}(^4G)$	3.23				
	$^6A_{1g}(^6S)\rightarrow{}^4E_g(^4D)$		3.32	3.36	3.76	
E_7	$2(^6A_{1g}(^6S))\rightarrow{}^4T_{1g}(^4G)+{}^4A_{1g}, {}^4E_g(^4G)$	3.95				
	$^6A_{1g}(^6S)\rightarrow{}^4T_{1g}(^4D)$		3.7	3.88		3.76-4.0
		B=699 cm^{-1} Dq= cm^{-1}	B=660 cm^{-1} Dq= 1510 cm^{-1}	B=540 cm^{-1} Dq= 1400 cm^{-1}		

*) The energies of the absorption features were presented in Ref. [57] but their identification with the particular electron transitions was not made.

Concluding discussion on the MCD nature, one can make a statement that magneto-optical effects are determined mainly by the d-d transitions while optical absorption is associated primary with the charge transfer transitions. The last type of transitions occur from the ligand states which are nonmagnetic and therefore they are not sensitive to the circular light polarization [58].

References

[1] J. Kunz, Die magnetischen eigenschaften des hãmatits, Neues Jahrbuch fur Mineralogie **1**, 62 (1907).

[2] T. Smith, The magnetic properties of hematite, Phys. Rev. **8,** 721 (1916).

[3] T. Smith, Magnetization and hysteresis in hematite crystals, Phys. Rev. **15**, 345 (1920).

[4] F.J. Morin, Magnetic susceptibility of a-Fe_2O_3 and a-Fe_2O_3 with added titanium, Phys. Rev. **78**, 819 (1950).

[5] C.G. Shull, W.A. Strauser, E.O. Wollan, Neutron diffraction by paramagnetic and antiferromagnetic substances, Phys. Rev. **83**, 333 (1951).

[6] I.E. Dzialoshinskii, Thermodynamic theory of "weak" ferromagnetism in antiferromagnetic substances, J. Exp. Theor. Phys. **32** 1547-1562, (1957). Soviet Physics JETP, **5**, 1259 (1957).

[7] O. Ozdemir, D.J. Dunlop, T.S. Berquo, Morin transition in hematite: Size dependence and thermal hysteresis, Geochemistry, Geophysics, Geosystems **9**, Q10Z01 (2008).

[8] M.A. Chueva, I.N. Mishchenko, S.P. Kubrin, T. A. Lastovina, Novel Insight into the Effect of Disappearance of the Morin Transition in Hematite Nanoparticles, Pis'ma v Zh.Eksp. i Teor. Fiz. **105**, 668 (2017), JETP Lett. **105**, 700 (2017).

[9] S.V. Ovsyannikov, N.V. Morozova, A.E. Karkin, V.V. Shchennikov, High-pressure cycling of hematite α-Fe_2O_3: Nanostructuring, in situ electronic transport, and possible charge disproportionation, Phys. Rev. B **86**, 20513 (2012).

[10] H. Zhou, C. Yuan, Z. An, Y. Yang, K. Xu, T. Yu, X. Luo, Strain-induced phase-structure of Fe_2O_3 nanoparticles, J. All. Com. **742**, 7 (2018).

[11] G.M. da Costa, E. Van San, E. De Grave, R.E. Vandenberghe, V. Barron, I. Datas, Al hematites prepared by homogeneous precipitation of oxinates: material characterization and determination of the Morin temperature, Phys. Chem. Mater. **29**, 122 (2002).

[12] D.M. Sherman and T.D. Waite, Electronic spectra of Fe^{3+} oxides and oxide hydroxides in the near IR to UV, American Mineralogist **70**, 1262 (1985).

[13] R.G.J. Strens, B.J. Wood, Diffuse reflectance spectra and optical properties of some iron and titanium oxides and oxyhydroxides, Mineralogical Magazine **43**, 347 (1979).

[14] Y. Tanabe, T. Moriya, S. Sugano, Magnon-induced electric dipole transition moment, Phys. Rev. Lett. **15**, 1023 (1965).

[15] L. Lu, L. Li, X. Wang, G. Li, Understanding of the Finite Size Effects on Lattice Vibrations and Electronic Transitions of nano α-Fe_2O_3, J. Phys. Chem. B **109**, 17151 (2005).

[16] Y.P. He, Y.M. Miao, C.R. Li, S.Q. Wang, L. Cao, S.S. Xie, G.Z. Yang, B.S. Zou, Size and structure effect on optical transitions of iron oxide nanocrystals, Phys. Rev. B **71**, 125411 (2005).

[17] S. Mitra, S. Das, K. Mandal, S. Chaudhuri, Synthesis of a α-Fe_2O_3 nanocrystal in its different morphological attributes: growth mechanism, optical and magnetic properties, Nanotechnology **18**, 275608 (2007).

[18] S. Chakrabarty, K.Chatterjee, Oriented growth of α-Fe_2O_3 nanocrystals with different morphology and their optical behavior, J. Cryst. Growth **381**, 107 (2013).

[19] L.A. Marusak, R. Messier and W.B. White, Optical absorption spectrum of hematite α-Fe_2O_3 in near IR to UV, J. Phys. Chem. Sol. **41**, 981 (1980).

[20] I. Jõgi, T.J. Jacobsson, M. Fondell, T. Wätjen, J.-O. Carlsson, M. Boman, T. Edvinsson, Phase Formation Behavior in Ultrathin Iron Oxide, Langmuir **31**, 12372 (2015).

[21] S. Piccinin, The band structure and optical absorption of hematite (alpha-Fe_2O_3): a first-principles GW-BSE study, Phys. Chem. Chem. Phys. **21**, 2957 (2019).

[22] H.J. Williams, R.C. Sherwood, J.P. Remeika, Magnetic domains in α-Fe_2O_3, J. Appl. Phys. **29**, 1772 (1958).

[23] E. Appel, V. Hoffmann, H.C. Soffel, Magneto-optical Kerr effect in (titano) magnetite, pyrrhotite and hematite, Phys. Earth and Planetary Interiors **65**, 36 (1990).

[24] P. Hejda, V. Kropáeek, E. Petrovsky, T. Zelinka, J. Zatecky, Some magnetic properties of synthetic and natural hematite of different grain size, Phys. Earth and Planetary Interiors **70**, 261 (1992).

[25] R.V. Pisarev, I.G. Sinii, G.A Smolenskii. Turning of Magnetic Sublattices and Anomalies of the Cotton-Mouton Effect in Terbium Iron Garnet and in Hematite, ZhETF Pisma **9**, 294 (1969).

[26] G.A. Smolenskii, R.V. Pisarev, I.G. Sinii, Birefringence of light in magnetically ordered crystals, Uspehi Fizicheskih Nauk **116**, 231-270 (1975). Translated in Sov. Phys. Usp. **18**, 410 (1975).

[27] I.Sh. Akhmadullin, V.A. Golenishchev-Kutuzov, S.A. Migachev, M F. Sadykov, Magnetic Birefringence of Light in Hematite, Fizika Tverdogo Tela **44**, 321 (2002), translated in Phys. Sol. St. **4**, 333 (2002).

[28] G.S. Krinchik, A.P. Khrebtov, A.A. Askochenskii, V.E. Zubov, Surface magnetism of hematite, ZhETF Pis. 17, 466 (1973).

[29] G.S. Krinchik, A.P. Khrebtov, A.A. Askochenski, E.M. Speranskaya, S.A. Belyaev, Magneto-optical spectra of 3d ions in spinel ferrites and weak ferromagnets, Zh. Eksp. Teor. Fiz. **72**, 699 (1977).

[30] V.E. Zubov, G.S. Krinchik, V.A. Lyskov, Magneto-optical properties of hematite, Zh. Eksp. Teor. Fiz. **81**, 1489 (1981).

[31] S. Balasubramanian, R. Panmand, G. Kumar, S.M. Mahajan, B.B. Kale, Magneto-Optic evaluation of antiferromagnetic α-Fe_2O_3 nanoparticles coated on a quartz substrate, Proceedings of SPIE **9758**, 97580O (2016).

[32] Bruker AXS TOPAS V4: General profile and structure analysis software for powder diffraction data. – User's Manual. Bruker AXS, Karlsruhe, Germany. 2008.

[33] R. Ivantsov, N. Evsevskaya, S. Saikova, E. Linok, G. Yurkina, I. Edelman, Synthesis and characterization of $Dy^3Fe^5O^{12}$ nanoparticles fabricated with the anion resin exchange precipitation method, J. Mater. Sci. ENG. B **226**, 171 (2017).

[34] S. V. Rykhlitskii, V. A. Shvets, E. V. Spesivtsev, V. Yu. Prokop'ev, S. G. Ovchinnikov, V. N. Zabluda, N. N. Kosyrev, S. N. Varnakov, and D. V. Shevtsov, Prib. Tekh. Eksp. **2**, 165 (2012).

[35] O.A. Maximova, N.N. Kosyrev, S.N. Varnakov, S.A. Lyaschenko, I.A. Yakovlev, I.A. Tarasov, D.V. Shevtsov, O.M. Maximova, S.G. Ovchinnikov. In situ magneto-optical ellipsometry data analysis for films growth control, J.M.M.M. **440**, 196 (2017).

[36] O.I. Bakradze, An ellipsometric method for measuring the parameters of thin magnetic films, Journal of Optical Technology **72**, 225 (2005).

[37] J. Hua, J. Gengsheng, Hydrothermal synthesis and characterization of mono-disperse α-Fe_2O_3 nanoparticles, Mater. Lett. **63**, 2725 (2009).

[38] T. Almeida, M. Fay, Y.Q. Zhu, P.D. Brown, Process map for the hydrothermal synthesis of α-Fe_2O_3 nanorods, J. Phys. Chem. C **113**, 18689 (2009).

[39] Mustehsin Ali, U. Tehseen, M. Ali, L. Ali, M. Mumtaz, Stugy of uncoated and silica-coated (α-Fe_2O_3) nanoparticles, Surfaces and interfaces **13**, 196 (2018).

[40] Powder Diffraction File (PDF 4+, 2018): Inorganic Phases (International Center for Diffraction Data, Swarthmore, Pennsylvania, United States, 2018).

[41] M. Hanesch, Raman spectroscopy of iron oxides and (oxy)hydroxides at low laser power and possible applications in environmental magnetic studies, Geophys. J. Int. **177**, 941 (2009).

[42] L. Yu. Novoselova, Hematite nanoparticle clusters with remarkably high magnetization synthesized from water treatment waste by one-step “sharp high temperature dehydration, RSC Adv. **7**, 51298 (2017).

[43] A. Lassoued, B. Dkhil, A. Gadri, S. Ammar, Control of the shape and size of iron oxide (alpha-Fe_2O_3) nanoparticles synthesized through the chemical precipitation method, Results in physics **7**, 3007 (2017).

[44] I.V. Chernyshova, M.F. Hochella and A.S. Madden, Size-dependent structural transformations of hematite nanoparticles. 1. Phase transition, Phys. Chem. Chem. Phys. **9**, 1736 (2007).

[45] D.L.A. de Faria, S. Venancio Silva and M.T. de Oliveira, Raman Microspectroscopy of Some Iron Oxides and Oxyhydroxides, Journal of Raman spectroscopy **28**, 873È878 (1997).

[46] G.B. Scott, D. E. Lacklison, H. I. Ralph, and J. L. Page, Magnetic circular dichroism and Faraday rotation spectra of $Y_3Fe_5O_{12}$, Phys. Rev. B **12**, 2562 (1975).

[47] I.Edelman, O. Ivanova, R. Ivantsov, D. Velikanov, V. Zabluda, Y. Zubavichus, A. Veligzhanin, V. Zaikovskiy, S. Stepanov, A. Artemenko, J. Curély and J. Kliava, Magnetic nanoparticles formed in glasses co-doped with iron and larger radius elements, J. Appl. Phys. **112**, 084331 (2012).

[48] F.J. Kahn, P.S. Pershan, J. P. Remeika, Ultraviolet Magneto-Optical Properties of Single-Crystal Orthoferrites, Garnets, and Other Ferric Oxide Compounds, Phys. Rev. **186**, 891 (1969).

[49] M. Lenglet, F. Hochu, and Z. Simsa, Covalency of Fe^{3+}–O^{2-} bonds and magnetic structure in mixed oxides, Mater. Res. Bull. **33**, 1821 (1998).

[50] J. Ferguson, H.J. Guggenheim, and Y. Tanabe, The origins of the colours of natural yellow, blue, and green sapphires, Phys. Soc. Jpn. **21**, 347 (1966).

[51] J.J. Krebs and W. G. Maisch, Exchange Effects in the Optical-Absorption Spectrum of Fe^{3+} in Al_2O_3, Phys. Rev. B **4**, 757 (1971).

[52] J. Tauc, Optical properties and electronic structure of amorphous Ge and Si, Mater. Res. Bull. **3**, 37 (1968).

[53] B.K. Pandey, A.K. Shahi, J. Shah, R.K. Kotnala, R. Gopal, Optical, magnetic and thermal properties of colloidal suspension of ferrofluids synthesized by laser ablation, Mater. Res. Express **4**, 075001 (2017)

[54] P. Chen, N. Lee, S. McGill, S.-W. Cheong, and J. L. Musfeldt, Magnetic-field-induced color change in α-Fe_2O_3 single crystals, Phys. Rev. B **85**, 174413 (2012).

[55] C. T. Chen and B. D. Cahan, Visible and ultraviolet optical properties of single-crystal and polycrystalline hematite measured by spectroscopic ellipsometry, J. Opt. Soc. Am. **71**, 932 (1981).

[56] A. I. Galuza, V. V. Eremenko and A. I. Kirichenko, Kramers-Kronig analysis of reflection spectra of hematite, Sov. Phys.Solid State **21**, 654 (1979).

[57] A.K. Ramasami, T.N. Ravishankar, K. Sureshkumar, M.V. Reddy, B.V.R. Chowdari, T. Ramakrishnappa, G.R. Balakrishna, Synthesis, exploration of energy storage and electrochemical sensing properties of hematite nanoparticles, Journal of Alloys and Compounds **671**, 552 (2016).

[58] A.V. Malakhovskii, A.L. Sukhachev, A.D. Vasil’ev, A.A. Leont’ev, A.V. Kartashev, V.L. Temerov, and I.A. Gudim, Nature of optical properties of $GdFe_3(BO_3)_4$ and $GdFe_{2.1}Ga_{0.9}(BO_3)_4$ crystals and other $3d^5$ antiferromagnets, Eur. Phys. J. B **85**, 80 (2012).